Aerospace Science and Technology 58 (2016) 36–47

Contents lists available at ScienceDirect

Aerospace Science and Technology

www.elsevier.com/locate/aescte

An improved extended Kalman filter with inequality constraints for gas turbine engine health monitoring

Feng Lu [a,b,*], Hongfei Ju [a,c], Jinquan Huang [a]

[a] Jiangsu Province Key Laboratory of Aerospace Power Systems, College of Energy and Power Engineering, Nanjing University of Aeronautics and Astronautics, Nanjing, 210016, PR China
[b] Department of Mechanical and Industrial Engineering, University of Toronto, Toronto, ON, M5S 3G8, Canada
[c] Aviation Motor Control System Institute, Aviation Industry Corporation of China, Wuxi 214063, PR China

ARTICLE INFO

Article history:
Received 4 November 2015
Received in revised form 24 July 2016
Accepted 9 August 2016
Available online 12 August 2016

Keywords:
Gas turbine engine
Health monitoring
Extended Kalman filter
Underdetermined estimation
Inequality constraint
Truncated probability density function

ABSTRACT

Various Kalman filter approaches have been proposed for the state estimation of gas turbine engines, among which Linear Kalman Filter (LKF) is the most common one. Kalman filters achieve state estimation provided that there are more available measurement sensors than state parameters to be estimated. However, it is hard to hold this assumption in gas turbine engine health monitoring applications, and an underdetermined estimation problem rises up.

The aim of this contribution is to present a nonlinear underdetermined state estimation method on the basis of Extended Kalman Filter (EKF); and to evaluate the performance of this methodology, the comparisons of three nonlinear estimators, i.e. basic EKF, underdetermined EKF and resultant EKF are conducted to gas turbine engine health state estimation. The underdetermined EKF is developed from the previous linear achievements using the transformation matrix, and it produces the least estimation errors in the nonlinear framework. Moreover, the prior state information represented by inequality constraints is introduced to create the resultant EKF, and the estimates of state variables are tuned to truncated Probability Density Function (PDF). Results from the application to a turbojet engine health monitoring in the flight envelope show that the proposed methodology yields a significant improvement in terms of underdetermined estimation accuracy and robustness.

1. Introduction

Gas turbine engine provides power for airplane, and reliable and efficient operation is important to flight safety and performance. With the demand on more reliability and low maintenance cost, engine health monitoring has received a wide interest [1,2]. The information about engine health state is used by flight crew and ground maintenance groups for further decision, and it should be accurate and reliable. Engine component health parameters like efficiencies and flow capacities are generally employed to represent gas turbine engine health states [3,4]. Since these health parameters are unmeasurable, the sensor measurements are collected and used to estimate health parameters. Various approaches have been proposed for engine health estimation, such as Kalman filter [5,6], least square algorithm [7], Bayesian hierarchical models [8,9], neural network [10,11], fuzzy logic [12], frequency domain analysis [13] and stochastic data fusion [14,15]. Among these methods, Kalman filter has been paid the most attention due to easy achievement recently, and it is one of model-based state estimation methods relying on physical characteristics of gas turbine engine.

Kalman filter is a minimum-variance state estimator for dynamic system with Gaussian noise, and the overall architecture of turbojet engine health monitoring using Kalman filter is shown in Fig. 1 [5]. The engine control system usually doesn't contain the health monitoring module, but it provides real-time data to the module for state estimation during engine steady operation. Among the variants of Kalman filter, the Linear Kalman Filter (LKF) is widely used for gas turbine engine health estimation and performance prognosis [16,17]. The LKF closely depends on the State Variable Model (SVM), which is a classic linear model developed and simplified from nonlinear aero-thermodynamic model of gas turbine engine [18]. For the LKF application, we need to build a number of steady base model and SVMs at these steady operating points at first. It is noted that the SVM and LKF are designed in the linear framework, and they are effective only in a small range

* Corresponding author at: Jiangsu Province Key Laboratory of Aerospace Power Systems, College of Energy and Power Engineering, Nanjing University of Aeronautics and Astronautics, Nanjing, 210016, PR China. Fax: +86 25 848 93666.
E-mail address: lufengnuaa@126.com (F. Lu).

http://dx.doi.org/10.1016/j.ast.2016.08.008
1270-9638/

Nomenclature

PDF	Probability Density Function
EHM	Engine health management
LKF	Linear Kalman Filter
EKF	Extended Kalman Filter
SVM	State Variable Model
LPC	Low Pressure Compressor
HPC	High Pressure Compressor
HPT	High Pressure Turbine
LPT	Low Pressure Turbine
$\boldsymbol{A}, \boldsymbol{C}, \boldsymbol{L}, \boldsymbol{M}, \boldsymbol{T}, \boldsymbol{W}, \boldsymbol{S}, \boldsymbol{I}$	Proper dimension matrices
$\boldsymbol{P}, \boldsymbol{Q}, \boldsymbol{R}$	Covariance matrices
$\boldsymbol{K}$	Kalman gain matrix
$\boldsymbol{V}$	Transformation matrix
$\boldsymbol{o}_c$	Control input vector
$\boldsymbol{x}$	State vector
$\boldsymbol{y}$	Vector of measured outputs
$\boldsymbol{w}$	Vector of process inaccuracies
$\boldsymbol{v}$	Vector of measurement inaccuracies
$\boldsymbol{z}$	Intermediate state vector
$\boldsymbol{h}$	Health parameter vector
$\boldsymbol{q}$	Tuning vector
f, g	Nonlinear function
P_{25}	LPC outlet pressure
P_3	HPC outlet pressure
P_{45}	HPT outlet pressure
P_6	LPT outlet pressure
T_{45}	HPT outlet temperature
T_6	LPT outlet temperature
N_L	Low pressure spool speed
N_H	High pressure spool speed
SE_1	LPC efficiency
SE_2	HPC efficiency
SE_3	HPT efficiency
SE_4	LPT efficiency
SW_1	LPC flow capacity
SW_2	HPC flow capacity
SW_3	HPT flow capacity
SW_4	LPT flow capacity
ME	Root mean square error
SD	Standard square error

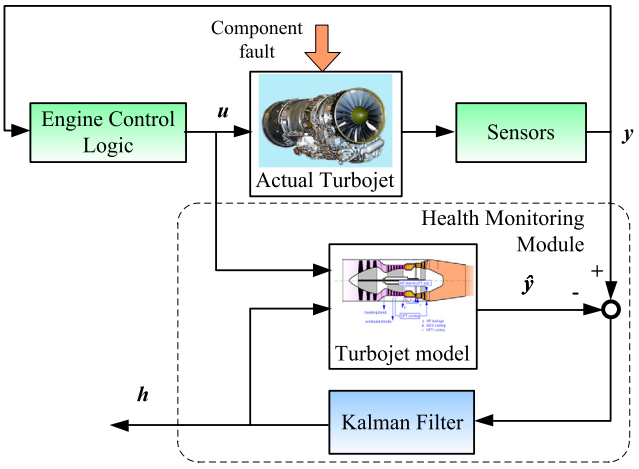

Fig. 1. Turbojet engine health monitoring based on Kalman filter.

around the steady operating point. Considering gas turbine engine is a nonlinear dynamic system, the LKF performance would decrease sharply as the engine leaves far from the steady operating point. Hence, a nonlinear state estimation, like Extended Kalman Filter (EKF), Unscented Kalman Filter and Particle Filter, might be more potential for engine health monitoring [19].

The sensor to measure speed, temperature and pressure is installed for engine health evaluation, the count of which is limit due to the complex engine structure. Besides, some sensors tend to break down as seriously cruel operating condition of gas turbine engine. As a result, the available sensor might be less than health parameter to be estimated in health state estimation process, and it was defined by an underdetermined estimation problem. As was mentioned earlier, Kalman filter techniques could be used for the estimation of engine health parameters, but it is only achieved in the condition that the number of sensor measurements is more than the state variable count [20]. The solution to underdetermined estimation of the LKF is to introduce tuning parameter, which is a linear subset of the original health parameter. But wrong estimation results generate in some cases due to no enough available measured information [21]. Up to this point in time, a significant improvement in the LKF algorithm is proposed using an optimal transformation matrix for gas-path fault diagnosis [17]. In this paper, the tuning LKF is extended to the state estimation of nonlinear dynamic system at first, so-called the underdetermined EKF, and it is applied to turbojet engine health monitoring.

The underdetermined EKF can reach the state estimates using less sensor measurements compared to the basic EKF, but the reduction of sensed information used for state estimation will be negative to the underdetermined EKF performance. In order to make up for the missing sensed information, the known health condition that is usually ignored in the basic EKF is employed to the nonlinear estimator in this paper, and it is represented in the forms of inequality constraints. For nonlinear dynamic system, resultant EKF is developed from underdetermined EKF with inequality constraints using truncated Probability Density Function (PDF) to improve health state estimation performance. The experiments to evaluate the estimation accuracy and robustness of the proposed methodologies are performed at the maximum operating point in various flight regions. The experimental results are in favor of our viewpoints.

The roadmap of this paper is as follows. A nonlinear dynamic model of turbojet engine is given, and the nonlinear underdetermined estimation problem is generalized in Section 2. Section 3 briefly reviews the basic EKF, and then develops nonlinear underdetermined estimation algorithms, i.e. underdetermined EKF and resultant EKF. Section 4 presents experimental comparisons of nonlinear state estimation methods performed on the examined engine. In Section 5, conclusions and future research directions are drawn.

2. Problem formulation

Gas turbine engine mechanical fatigue fracture, erosion, corrosion and foreign-object damage cause the deviations of engine component thermodynamic maps. The efficiency and flow capacity variations from their normal values in the maps are commonly recognized as engine gas path health performance anomaly. These health parameters can be worked out from the measurements using state estimator, and the linear estimator LKF has limitation in application discussed earlier. Then the higher order linearization or nonlinear estimation methods are studied. Previous publica-

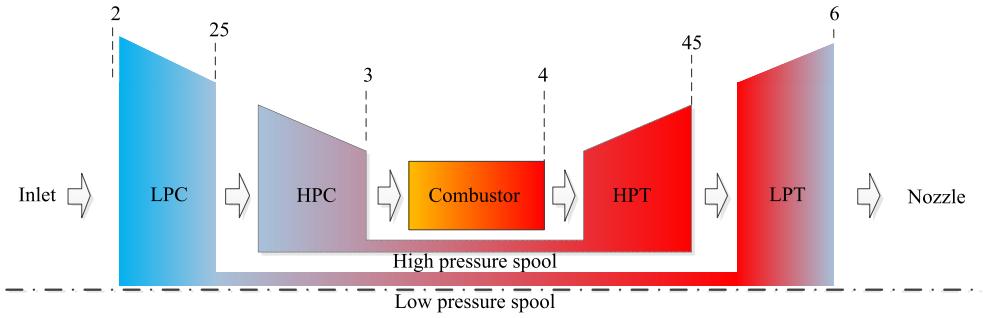

Fig. 2. Schematic representation of a two-spool turbojet engine.

Table 1
Gas turbine engine performance deterioration over time.

Cycle	ΔSE_1	ΔSW_1	ΔSE_2	ΔSW_2	ΔSE_3	ΔSW_3	ΔSE_4	ΔSW_4
0	0	0	0	0	0	0	0	0
3000	−1.5%	−2.04%	−2.94%	−3.91%	−2.63%	1.76%	−0.54%	0.26%
4500	−2.18%	−2.85%	−6.71%	−8.99%	−3.22%	2.17%	−0.81%	0.34%
6000	−2.85%	−3.65%	−9.40%	−14.06%	−3.81%	2.57%	−1.08%	0.42%

tion [19] indicates that gas turbine engine nonlinearities are mild enough, and the EKF is the most proper candidates for engine health estimation in terms of estimation accuracy and computational efforts compared to LKF and unscented Kalman filter. Hence, the following researches focus on the EKF framework.

A turbojet engine as an important kind of aircraft gas turbine is studied and illustrated in Fig. 2. The engine includes inlet, low pressure compressor (LPC), high pressure compressor (HPC), combustor, high pressure turbine (HPT), low pressure turbine (LPT) and nozzle [22–24]. The inlet supplies airflow into the LPC, then the air passes through the HPC and moves to the combustor. Fuel is injected and hot gas is produced in the combustor for driving the turbines. The HPC and LPC are driven by the HPT and LPT, respectively. The gas leaves the engine through the nozzle. The engine station numbers in Fig. 2 are as follows, inlet exit marked by 2, LPC exit by 25, HPC exit by 3, combustor exit by 4, HPT exit by 45, LPT exit by 6.

The proposed methodology is tested on nonlinear dynamic mathematical model of the turbojet engine created from engine component level model, which is based on aero-thermodynamic physical theory [18,25–27]. It is coded with C language and packaged by Dynamic Link Library (DLL) for simulation in Matlab environment [28,29]. The cycle frequency of the engine CLM is 100 Hz, and the update rate of engine health estimation system is 50 Hz. The nonlinear model of turbojet engine is described as follows

$$\begin{aligned} \boldsymbol{x}_{k+1} &= \boldsymbol{f}(\boldsymbol{x}_k, \boldsymbol{u}_k, \boldsymbol{o}_{c,k}) + \boldsymbol{w}_k \\ \boldsymbol{y}_k &= \boldsymbol{g}(\boldsymbol{x}_k, \boldsymbol{u}_k, \boldsymbol{o}_{c,k}) + \boldsymbol{v}_k \end{aligned} \tag{1}$$

where k is the time index, $\boldsymbol{x}$ is a 10-element augmented state vector, $\boldsymbol{u}$ is a 2-element control input, $\boldsymbol{o}_c$ is a 2-element flight condition input, and $\boldsymbol{y}$ is a 8-element measured output. The noise terms $\boldsymbol{w}_k$ and $\boldsymbol{v}_k$ separately represent process inaccuracies and measurement inaccuracies, and follow the time-uncorrelated zero-mean white noise. The elements of control vector in the nonlinear dynamic model are fuel flow W_f and nozzle area A_8. The flight condition variables include altitude H and Mach number Ma. The sensor measurements consist of LPC outlet pressure P_{25}, HPC outlet pressure P_3, HPT outlet pressure P_{45}, LPT outlet pressure P_6, HPT outlet temperature T_{45}, LPT outlet temperature T_6, low pressure spool speed N_L and high pressure spool speed N_H. The augmented state vector x contains two original state variables (N_L and N_H) and eight health parameters (LPC efficiency SE_1, HPC efficiency SE_2, HPT efficiency SE_3, LPT efficiency SE_4, LPC flow capacity SW_1, HPC flow capacity SW_2, HPT flow capacity SW_3, LPT flow capacity SW_4). The engine health status is represented by health parameter variations $\Delta \boldsymbol{h} = [\Delta SE_1, \Delta SW_1, \Delta SE_2, \Delta SW_2, \Delta SE_3, \Delta SW_3, \Delta SE_4, \Delta SW_4]^T$, which are defined as follows

$$\begin{aligned} \Delta SE_i &= \frac{SE_i}{SE_i^*} - 1 \qquad i = 1, 2, 3, 4 \\ \Delta SW_j &= \frac{SW_j}{SW_j^*} - 1 \quad j = 1, 2, 3, 4 \end{aligned} \tag{2}$$

where SE_i^* is the normal value of the ith health parameter. We can estimate both original state variables and health parameters by the EKF provided all sensors operate normally and their measurements are well collected. If one sensor breaks down, the available sensed signal number for engine health estimation is reduced, e.g. the available measurement vector will become to $\boldsymbol{y} = [N_L, N_H, P_{25}, P_{45}, T_{45}, P_6, T_6]^{\mathrm{T}}$ as sensor P_3 failure occurs. The number of sensed data is seven, while the number of health parameters still eight. Then the underdetermined estimation issue emerges, and the basic EKF fails to deal with it. It is necessary to draw forth a novel nonlinear estimator to underdetermined estimation.

In addition, both the engine performance deterioration and performance faults could cause health parameter shift, and finally result in engine performance anomaly. The health parameter variation resulted from deterioration is a long-term and usually larger than that from fault [30,31]. Table 1 shows gas turbine engine performance deterioration during the course of its lifetime, and the engine component efficiency and flow capacity diverges from the nominal quantities with the cycle number increase [30,32].

It can be seen from Table 1 that health parameters vary various values at the same cycle number, and there are different drift ways of health parameters as performance deterioration. The health parameters ΔSW_3 and ΔSW_4 move in positive direction while the remaining ones in negative direction. It is noted that the variation of each health parameter is finite within a specific range in both cases of performance deterioration and fault [31]. These fixed variation scopes of health parameters could be recognized as significant prior state information, and are employed to determine the inequality constraints in this study. Define the upper limit value

and lower limit value of the ith health parameter $\boldsymbol{h}_i$ as $\boldsymbol{b}_i$ and $\boldsymbol{a}_i$, then the inequalities related to the ith health parameters follow

$$\begin{cases} \boldsymbol{h}_{i,k} \le \boldsymbol{b}_i \\ \boldsymbol{h}_{i,k} \ge \boldsymbol{a}_i \end{cases} \quad i = 1, \cdots, 8 \tag{3}$$

Since the quantity of health parameter deviation caused by performance deterioration at the last cycle number is larger than that by performance fault, the constrained bounds are referred to the maximum performance deterioration value of health parameter at 6000 cycle number in Table 1. The upper and lower limit vectors are separately $\boldsymbol{b} = [1.01, 1.01, 1.01, 1.01, 1.01, 1.03, 1.01, 1.01]^T$, $\boldsymbol{a} = [0.97, 0.96, 0.90, 0.85, 0.96, 0.99, 0.98, 0.99]^T$ after adding small quantity tolerant bands. For example, ΔSW_1 is 0% initially and −3.65% at 6000 cycle number in Table 1, then the upper and lower bounds of SW_1 are 1.01 and 0.96. These bound values are corresponding to the second element of constraint bound vectors $\boldsymbol{b}$ and $\boldsymbol{a}$, respectively. The inequality constraints are often neglected in conventional EKF algorithm. This paper tries to develop a way to nonlinear underdetermined estimation issue with inequality constraints of state variable, and proofs that the proposed methodology improves the estimation accuracy in turbojet engine health monitoring applications.

3. Nonlinear estimation algorithms for health monitoring

3.1. Extended Kalman filter

In the EKF algorithm, Taylor rules are adopted to expand the nonlinear dynamic system around a nominal operating point, and system matrices are calculated by Jacobian calculations [19]. The EKF algorithm for state estimation of the nonlinear dynamic system as Eq. (1) is given

$$\begin{aligned} \boldsymbol{x}_k^- &= \boldsymbol{f}(\boldsymbol{x}_{k-1}, \boldsymbol{u}_{k-1}, \boldsymbol{o}_{c,k-1}) \\ \boldsymbol{P}_k^- &= \boldsymbol{A}\boldsymbol{P}_{k-1}\boldsymbol{A}^T + \boldsymbol{Q} \\ K_k &= \boldsymbol{P}_k^-\boldsymbol{C}^T\left(\boldsymbol{C}\boldsymbol{P}_k^-\boldsymbol{C}^T + \boldsymbol{R}\right)^{-1} \\ \boldsymbol{x}_k &= \boldsymbol{x}_k^- + \boldsymbol{K}_k\left[\boldsymbol{y}_k - \boldsymbol{g}\left(\boldsymbol{x}_k^-, \boldsymbol{u}_{k-1}, \boldsymbol{o}_{c,k-1}\right)\right] \\ \boldsymbol{P}_k &= (\boldsymbol{I} - \boldsymbol{K}_k\boldsymbol{C})\boldsymbol{P}_k^- \end{aligned} \tag{4}$$

where $\boldsymbol{Q}$ denoted the covariance of process noise $\boldsymbol{w}$, and $\boldsymbol{R}$ denoted the covariance of measurement noise $\boldsymbol{v}$. The system matrices $\boldsymbol{A}$ and $\boldsymbol{C}$ are obtained as follows

$$\begin{aligned} \boldsymbol{A} &= \begin{pmatrix} \boldsymbol{A}_r & \boldsymbol{L}_h \\ \boldsymbol{0} & \boldsymbol{I} \end{pmatrix} = \frac{\partial \boldsymbol{f}(\boldsymbol{x}_{k-1}, \boldsymbol{u}_{k-1}, \boldsymbol{o}_{c,k-1})}{\partial \boldsymbol{x}_{k-1}} \\ \boldsymbol{C} &= \begin{pmatrix} \boldsymbol{C}_r & \boldsymbol{M}_h \end{pmatrix} = \frac{\partial \boldsymbol{g}(\boldsymbol{x}_{k-1}, \boldsymbol{u}_{k-1}, \boldsymbol{o}_{c,k-1})}{\partial \boldsymbol{x}_{k-1}} \end{aligned} \tag{5}$$

As was mentioned earlier, the augmented state vector $\boldsymbol{x} = [\boldsymbol{x}_r^T, \boldsymbol{h}^T]^T = [N_L, N_H, SE_1, SW_1, SE_2, SW_2, SE_3, SW_3, SE_4, SW_4]^T$ includes the original state variables and health parameters, and then the system matrices $\boldsymbol{A} \in \boldsymbol{R}^{10\times10}$, $\boldsymbol{C} \in \boldsymbol{R}^{8\times10}$ can be decomposed to the proper dimension sub-matrices $\boldsymbol{A_r} \in \boldsymbol{R}^{2\times2}$, $\boldsymbol{L_h} \in \boldsymbol{R}^{2\times8}$, $\boldsymbol{I} \in \boldsymbol{R}^{8\times8}$, $\boldsymbol{C_r} \in \boldsymbol{R}^{8\times2}$, $\boldsymbol{M_h} \in \boldsymbol{R}^{8\times8}$. The general EKF can't be achieved state estimation when the sensor measurement number is less than the health parameter count [33,34].

3.2. Underdetermined EKF with inequality constraints

For the purpose of underdetermined estimation for nonlinear dynamic system, the underdetermined EKF algorithm is developed at first, and then the inequality constraints are added into the underdetermined EKF to create resultant EKF. The key of the underdetermined EKF is to introduce a new reduced-order state vector so-called tuner $\boldsymbol{q} \in \boldsymbol{R}^m$, which is a linear combination of the original health parameter vector $\boldsymbol{h} \in \boldsymbol{R}^n$. The tuning vector $\boldsymbol{q}$ is expressed as follows

$$\boldsymbol{q} = \boldsymbol{V}\boldsymbol{h} \tag{6}$$

where $\boldsymbol{V}$ is a transformation matrix with rank m, and the tuner dimension m is less than that of health state vector n, i.e. $m < n$. An optimal transformation matrix with the minimum of estimation error is $\boldsymbol{V}^*$, and the Eq. (6) can also be written as $\Delta\boldsymbol{h} = (\boldsymbol{V}^*)^{-1}\Delta\boldsymbol{q}$ where $(\boldsymbol{V}^*)^{-1}$ is the pseudo-inverse of $\boldsymbol{V}^*$. When the tuner replaces the original health parameter vector, the augmented state vector becomes $\boldsymbol{x}_a = [\boldsymbol{x}_r^T, \boldsymbol{q}^T]^T$. In order to prevent convergence to a poorly scaled solution, transformation matrix follows $\|\boldsymbol{V}^*\|_F = 1$ (F is the Frobenius norm) [16,20].

Given that the nonlinear system runs in an open-loop process, flight condition vector and the control vector are constant ($\Delta\boldsymbol{u}_k = \boldsymbol{0}$, $\Delta\boldsymbol{o}_{c,k} = \boldsymbol{0}$), an approximation of new reduced-order augmented state variables $\Delta\hat{\boldsymbol{x}}_{a,k}$ at time k in the framework of EKF is formulated

$$\begin{aligned} &\Delta\hat{\boldsymbol{x}}_{a,k+1} = \boldsymbol{A}_a\Delta\hat{\boldsymbol{x}}_{a,k} + \boldsymbol{K}(\Delta\boldsymbol{y}_k - \boldsymbol{C}_a\boldsymbol{A}_a\Delta\hat{\boldsymbol{x}}_{a,k}) \\ &\boldsymbol{K} = \boldsymbol{P}\boldsymbol{C}_a^T\left(\boldsymbol{C}_a\boldsymbol{P}\boldsymbol{C}_a^T + \boldsymbol{R}\right)^{-1} \\ &\boldsymbol{P} = \boldsymbol{A}_a\boldsymbol{P}\boldsymbol{A}_a^T - \boldsymbol{A}_a\boldsymbol{P}\boldsymbol{C}_a^T\left(\boldsymbol{C}_a\boldsymbol{P}\boldsymbol{C}_a^T + \boldsymbol{R}\right)^{-1}\boldsymbol{C}_a\boldsymbol{P}\boldsymbol{A}_a^T + \boldsymbol{Q}_a \\ &\boldsymbol{Q}_a = \begin{pmatrix} \boldsymbol{I}_{2\times2} & \boldsymbol{0} \\ \boldsymbol{0} & \boldsymbol{V}^* \end{pmatrix}\boldsymbol{Q}\begin{pmatrix} \boldsymbol{I}_{2\times2} & \boldsymbol{0} \\ \boldsymbol{0} & \boldsymbol{V}^* \end{pmatrix}^T \end{aligned} \tag{7}$$

where the matrices with the subscript a are related to the state variables $\boldsymbol{x}_a$. The estimates of health parameter vector could be obtained from the tuner using the optimal transformation matrix

$$\begin{pmatrix} \Delta\hat{\boldsymbol{x}}_{r,k} \\ \Delta\hat{\boldsymbol{h}}_k \end{pmatrix} = \begin{pmatrix} \boldsymbol{I} & \boldsymbol{0} \\ \boldsymbol{0} & (\boldsymbol{V}^*)^{-1} \end{pmatrix}\Delta\hat{\boldsymbol{x}}_{a,k} \tag{8}$$

In the following section we will find the optimal transformation matrix $\boldsymbol{V}^*$ which produces the minimum of estimation error. Due to the inequality $\dim(\Delta\boldsymbol{q}) \le \dim(\Delta\boldsymbol{y}) < \dim(\Delta\boldsymbol{h})$, the tuner can't contain all information of the health parameters. Augmented state variable conversation where the tuner takes the place of the health parameter vector plays an important role in the estimation errors of the EKF.

$$\begin{pmatrix} \Delta\tilde{\boldsymbol{x}}_{r,k} \\ \Delta\tilde{\boldsymbol{h}}_k \end{pmatrix} = \begin{pmatrix} \Delta\hat{\boldsymbol{x}}_{r,k} \\ \Delta\hat{\boldsymbol{h}}_k \end{pmatrix} - \begin{pmatrix} \Delta\boldsymbol{x}_{r,k} \\ \Delta\boldsymbol{h}_k \end{pmatrix} \tag{9}$$

By taking expected values of both sides of Eq. (1), the nonlinear system model can be written as follows

$$\begin{aligned} &\begin{cases} E(\Delta\boldsymbol{x}_{k+1}) = E(f(\Delta\boldsymbol{x}_k, \Delta\boldsymbol{u}_k, \Delta\boldsymbol{o}_{c,k})) + E(\boldsymbol{w}_k) \\ E[\Delta\boldsymbol{y}_k] = E(g(\Delta\boldsymbol{x}_k, \Delta\boldsymbol{u}_k, \Delta\boldsymbol{o}_{c,k})) + E(\boldsymbol{v}_k) \end{cases} \\ &\Rightarrow \begin{cases} \Delta\bar{\boldsymbol{x}} = \begin{bmatrix} \Delta\bar{\boldsymbol{x}}_r \\ \Delta\bar{\boldsymbol{h}} \end{bmatrix} = \begin{bmatrix} \boldsymbol{A}_r & \boldsymbol{L}_h \\ \boldsymbol{0} & \boldsymbol{I} \end{bmatrix}\begin{bmatrix} \Delta\bar{\boldsymbol{x}}_r \\ \Delta\bar{\boldsymbol{h}} \end{bmatrix} \\ \Delta\bar{\boldsymbol{y}} = \begin{bmatrix} \boldsymbol{C}_r & \boldsymbol{M}_h \end{bmatrix}\begin{bmatrix} \Delta\bar{\boldsymbol{x}}_r \\ \Delta\bar{\boldsymbol{h}} \end{bmatrix} \end{cases} \\ &\Rightarrow \begin{cases} \Delta\bar{\boldsymbol{x}}_r = (\boldsymbol{I} - \boldsymbol{A}_r)^{-1}\boldsymbol{L}_h\Delta\bar{\boldsymbol{h}} \\ \Delta\bar{\boldsymbol{y}} = (\boldsymbol{C}_r(\boldsymbol{I} - \boldsymbol{A}_r)^{-1}\boldsymbol{L}_h + \boldsymbol{M}_h)\Delta\bar{\boldsymbol{h}} \end{cases} \end{aligned} \tag{10}$$

The expected values of reduced-order augmented state variables satisfy the following equations

$$\begin{aligned} &E[\Delta\hat{\boldsymbol{x}}_{a,k}] = \boldsymbol{A}_a E[\Delta\hat{\boldsymbol{x}}_{a,k-1}] + K\left(E[\Delta\boldsymbol{y}_k] - \boldsymbol{C}_a\boldsymbol{A}_a \cdot E[\Delta\hat{\boldsymbol{x}}_{a,k-1}]\right) \\ &\Delta\bar{\hat{\boldsymbol{x}}}_a = \boldsymbol{A}_a\Delta\bar{\hat{\boldsymbol{x}}}_a + \boldsymbol{K}(\Delta\bar{\boldsymbol{y}} - \boldsymbol{C}_a\boldsymbol{A}_a\Delta\bar{\hat{\boldsymbol{x}}}_a) \\ &\Delta\bar{\hat{\boldsymbol{x}}}_a = (\boldsymbol{I} - \boldsymbol{A}_a + \boldsymbol{K}\boldsymbol{C}_a\boldsymbol{A}_a)^{-1}\boldsymbol{K}\Delta\bar{\boldsymbol{y}} \end{aligned} \tag{11}$$

Thus, the mean state vector $\Delta\bar{\hat{\boldsymbol{x}}}_a$ in Eq. (12) can be defined

$$\Delta\bar{\hat{\boldsymbol{x}}}_a = (\boldsymbol{I} - \boldsymbol{A}_a + \boldsymbol{K}\boldsymbol{C}_a\boldsymbol{A}_a)^{-1}\boldsymbol{K}\left(\boldsymbol{C}_r(\boldsymbol{I} - \boldsymbol{A}_r)^{-1}\boldsymbol{L}_h + \boldsymbol{M}_h\right)\Delta\bar{\boldsymbol{h}} \tag{12}$$

By taking expected values of augmented state variable in Eq. (9), and we can reach the expected values of estimation errors

$$\begin{aligned}\begin{pmatrix}\Delta\bar{\hat{\boldsymbol{x}}}_r\\ \Delta\bar{\hat{\boldsymbol{h}}}\end{pmatrix} &= E\left[\begin{pmatrix}\Delta\hat{\boldsymbol{x}}_{r,k}\\ \Delta\hat{\boldsymbol{h}}_k\end{pmatrix}\right] - E\left[\begin{pmatrix}\Delta\boldsymbol{x}_{r,k}\\ \Delta\boldsymbol{h}_k\end{pmatrix}\right]\\ &= \begin{pmatrix}\boldsymbol{I} & \boldsymbol{0}\\ \boldsymbol{0} & (\boldsymbol{V}^*)^{-1}\end{pmatrix} E[\Delta\hat{\boldsymbol{x}}_{a,k}] - \begin{pmatrix}\Delta\bar{\boldsymbol{x}}_r\\ \Delta\bar{\boldsymbol{h}}\end{pmatrix}\\ &= \begin{pmatrix}\boldsymbol{I} & \boldsymbol{0}\\ \boldsymbol{0} & (\boldsymbol{V}^*)^{-1}\end{pmatrix} \Delta\bar{\hat{\boldsymbol{x}}}_a - \begin{pmatrix}\Delta\bar{\boldsymbol{x}}_r\\ \Delta\bar{\boldsymbol{h}}\end{pmatrix}\\ &= \boldsymbol{G}\Delta\bar{\boldsymbol{h}}\end{aligned} \tag{13}$$

where the matrix $\boldsymbol{G}$ can be calculated as follows

$$\begin{aligned}\boldsymbol{G} = &\begin{pmatrix}\boldsymbol{I} & 0\\ 0 & (\boldsymbol{V}^*)^{-1}\end{pmatrix}(\boldsymbol{I} - \boldsymbol{A}_a + \boldsymbol{K}\boldsymbol{C}_a\boldsymbol{A}_a)^{-1}\\ &\times \boldsymbol{K}\left(\boldsymbol{C}_r(\boldsymbol{I} - \boldsymbol{A}_r)^{-1}\boldsymbol{L}_h + \boldsymbol{M}_h\right)\\ &- \begin{pmatrix}(\boldsymbol{I} - \boldsymbol{A}_r)^{-1}\boldsymbol{L}_h\\ \boldsymbol{I}\end{pmatrix}\end{aligned} \tag{14}$$

From the Eq. (9), the mean square error takes the following form

$$\begin{aligned}\xi &= E\left[\begin{pmatrix}\Delta\bar{\hat{\boldsymbol{x}}}_r\\ \Delta\bar{\hat{\boldsymbol{h}}}\end{pmatrix}^T\begin{pmatrix}\Delta\bar{\hat{\boldsymbol{x}}}_r\\ \Delta\bar{\hat{\boldsymbol{h}}}\end{pmatrix}\right]\\ &= E\left[tr\left\{\begin{pmatrix}\Delta\bar{\hat{\boldsymbol{x}}}_r\\ \Delta\bar{\hat{\boldsymbol{h}}}\end{pmatrix}\begin{pmatrix}\Delta\bar{\hat{\boldsymbol{x}}}_r\\ \Delta\bar{\hat{\boldsymbol{h}}}\end{pmatrix}^T\right\}\right]\\ &= E\left[tr\left\{\boldsymbol{G}\Delta\bar{\boldsymbol{h}}\Delta\bar{\boldsymbol{h}}^T\boldsymbol{G}^T\right\}\right]\\ &= tr\left\{\boldsymbol{G}\boldsymbol{P}\boldsymbol{G}^T\right\}\end{aligned} \tag{15}$$

The difference of reduced-order augmented state variables estimates and their expect values satisfied

$$\begin{aligned}\boldsymbol{\varepsilon}_{a,k} &= \Delta\hat{\boldsymbol{x}}_{a,k} - E[\Delta\hat{\boldsymbol{x}}_{a,k}]\\ &= \Delta\hat{\boldsymbol{x}}_{a,k} - \Delta\bar{\hat{\boldsymbol{x}}}_a\\ &= (\boldsymbol{A}_a - \boldsymbol{K}\boldsymbol{C}_a\boldsymbol{A}_a)(\Delta\hat{\boldsymbol{x}}_{a,k-1} - \Delta\bar{\hat{\boldsymbol{x}}}_a) + \boldsymbol{K}(\Delta\boldsymbol{y}_k - \Delta\bar{\boldsymbol{y}})\\ &= (\boldsymbol{A}_a - \boldsymbol{K}\boldsymbol{C}_a\boldsymbol{A}_a)\boldsymbol{\varepsilon}_{a,k-1} + \boldsymbol{K}\boldsymbol{v}_k\end{aligned} \tag{16}$$

where $\boldsymbol{v}_k$ is defined by $\boldsymbol{v}_k = \Delta\boldsymbol{y}_k - \Delta\bar{\boldsymbol{y}}$, and $\boldsymbol{P}_{a,k}$ is the covariance matrix of $\boldsymbol{\varepsilon}_{a,k}$

$$\begin{aligned}&E\left[\boldsymbol{v}_k\boldsymbol{v}_k^T\right] = \boldsymbol{R}\\ &E\left[\boldsymbol{\varepsilon}_{a,k-1}\boldsymbol{v}_k^T\right] = E\left[\boldsymbol{v}_k\boldsymbol{\varepsilon}_{a,k-1}^T\right] = \boldsymbol{0}\\ &\boldsymbol{P}_{a,k-1} = E\left[\boldsymbol{\varepsilon}_{a,k-1}\boldsymbol{\varepsilon}_{a,k-1}^T\right]\end{aligned} \tag{17}$$

The matrix $\boldsymbol{P}_{a,k}$ related to the state vector $\boldsymbol{x}_a$ is calculated by solving the following equation

$$\begin{aligned}\boldsymbol{P}_{a,k} &= (\boldsymbol{A}_a - \boldsymbol{K}\boldsymbol{C}_a\boldsymbol{A}_a)E\left[\boldsymbol{\varepsilon}_{a,k-1}\boldsymbol{\varepsilon}_{a,k-1}^T\right](\boldsymbol{A}_a - \boldsymbol{K}\boldsymbol{C}_a\boldsymbol{A}_a)^T\\ &\quad + (\boldsymbol{A}_a - \boldsymbol{K}\boldsymbol{C}_a\boldsymbol{A}_a)E\left[\boldsymbol{\varepsilon}_{a,k-1}\boldsymbol{v}_k^T\right]\boldsymbol{K}^T\\ &\quad + \boldsymbol{K}E\left[\boldsymbol{v}_k\boldsymbol{\varepsilon}_{a,k-1}^T\right](\boldsymbol{A}_a - \boldsymbol{K}\boldsymbol{C}_a\boldsymbol{A}_a)^T\\ &\quad + \boldsymbol{K}E\left[\boldsymbol{v}_k\boldsymbol{v}_k^T\right]\cdot\boldsymbol{K}^T\\ &= (\boldsymbol{A}_a - \boldsymbol{K}\boldsymbol{C}_a\boldsymbol{A}_a)\boldsymbol{P}_{a,k-1}(\boldsymbol{A}_a - \boldsymbol{K}\boldsymbol{C}_a\boldsymbol{A}_a)^T + \boldsymbol{K}\boldsymbol{R}\boldsymbol{K}^T\\ &= (\boldsymbol{A}_a - \boldsymbol{K}\boldsymbol{C}_a\boldsymbol{A}_a)\boldsymbol{P}_{a,k}(\boldsymbol{A}_a - \boldsymbol{K}\boldsymbol{C}_a\boldsymbol{A}_a)^T + \boldsymbol{K}\boldsymbol{R}\boldsymbol{K}^T\end{aligned} \tag{18}$$

The covariance matrix $\boldsymbol{P}_{xh}$ about the original augmented state vector $\boldsymbol{x}$ can be calculated from Eq. (19)

$$\begin{aligned}\boldsymbol{P}_{xh,k} &= E\left[\left(\begin{pmatrix}\Delta\hat{\boldsymbol{x}}_{r,k}\\ \Delta\hat{\boldsymbol{h}}_k\end{pmatrix} - E\left[\begin{pmatrix}\Delta\hat{\boldsymbol{x}}_{r,k}\\ \Delta\hat{\boldsymbol{h}}_k\end{pmatrix}\right]\right)\right.\\ &\quad \left.\times\left(\begin{pmatrix}\Delta\hat{\boldsymbol{x}}_{r,k}\\ \Delta\hat{\boldsymbol{h}}_k\end{pmatrix} - E\left[\begin{pmatrix}\Delta\hat{\boldsymbol{x}}_{r,k}\\ \Delta\hat{\boldsymbol{h}}_k\end{pmatrix}\right]\right)^T\right]\\ &= \begin{pmatrix}\boldsymbol{I} & \boldsymbol{0}\\ \boldsymbol{0} & (\boldsymbol{V}^*)^{-1}\end{pmatrix}P_{a,k}\begin{pmatrix}\boldsymbol{I} & \boldsymbol{0}\\ \boldsymbol{0} & (\boldsymbol{V}^*)^{-1}\end{pmatrix}^T\end{aligned} \tag{19}$$

The estimation errors for the optimal transformation matrix include estimation mean deviation and square deviation, which are defined by the following equation and finally can be reached

$$\begin{aligned}e &= \xi + tr\{\boldsymbol{P}_{xh,k}\}\\ &= tr\left\{\boldsymbol{G}\boldsymbol{P}\boldsymbol{G}^T + \boldsymbol{P}_{xh,k}\right\}\end{aligned} \tag{20}$$

The health parameters are calculated from the tuning parameters by the optimal transformation matrix inverse $(\boldsymbol{V}^*)^{-1}$ in the underdetermined EKF, which produces the minimum estimation errors. The health parameter estimates can be achieved, while the available measurement number decrease inevitably affects the estimation accuracy of state variables by the underdetermined EKF.

In order to reduce uncertain estimation errors, the prior state information represented by inequality constraints is introduced to compensate partial absence of sensor measurements. For linear system, some studies had been carried out in the topics of state estimation with equality constraints, such as moving horizon estimation [35], estimate projection [36] and the smooth constrain [37]. When it comes to inequality constraint estimation, both hard and soft inequality constraint methods have been put forward to the LKF [38,39]. On the basis of the earlier achievements, the resultant EKF is developed and focused on uncertain estimation with inequality constraints for nonlinear dynamic system in this paper. The inequality constraints $\boldsymbol{a}_{i,k} \le \boldsymbol{h}_{i,k} \le \boldsymbol{b}_{i,k}$, $i = 1, \cdots, n$ is introduced into the underdetermined EKF, and it could be specified

$$\boldsymbol{a}_k \le \left(\boldsymbol{V}^*\right)^{-1}\boldsymbol{q}_k \le \boldsymbol{b}_k \tag{21}$$

To make this problem tractable, assume that these constraints are linearly independent, and the upper and lower bound values for each state variable are constant. We convert the original bound vectors $\boldsymbol{a}_k$ and $\boldsymbol{b}_k$ to reduced-order bound vectors $\boldsymbol{c}_k$ and $\boldsymbol{d}_k$

$$\begin{aligned}&\boldsymbol{V}^*\boldsymbol{a}_k \le \boldsymbol{q}_k \le \boldsymbol{V}^*\boldsymbol{b}_k\\ &\boldsymbol{c}_{j,k} \le \phi_{j,k}^T\boldsymbol{q}_k = \boldsymbol{q}_{j,k} \le \boldsymbol{d}_{j,k} \quad j = 1, \cdots, m\\ &\boldsymbol{c}_k = \boldsymbol{V}^*\boldsymbol{a}_k, \boldsymbol{d}_k = \boldsymbol{V}^*\boldsymbol{b}_k\end{aligned} \tag{22}$$

where $\boldsymbol{c}_{j,k}$ and $\boldsymbol{d}_{j,k}$ are the two sided constraints of the jth tuner element at time k, and $\phi_{j,k}^T$ is the former j row of the matrix ϕ_k ($\phi_k \in \boldsymbol{R}^{m\times m}$). The number of inequality constraints is totally m and also less than the original constraint number n after the state variable transformation.

With the tuner estimate $\hat{\boldsymbol{q}}_k$ and its covariance $\boldsymbol{Q}'_k$ at time k, the partial state estimates in underdetermined EKF hold the Gaussian probability density function (PDF) $N(\hat{\boldsymbol{q}}_k, \boldsymbol{Q}'_k)$. Once the inequality constraints Eq. (22) is considered in the underdetermined EKF, the PDF changes and then follows $N(\tilde{\boldsymbol{q}}_k, \tilde{\boldsymbol{Q}}'_k)$. The tuner estimate $\tilde{\boldsymbol{q}}_{j,k}$ and covariance $\tilde{\boldsymbol{Q}}'_{j,k}$ are defined after the former j scalar constraints enforced, and then the intermediate state variables $\boldsymbol{z}_{j,k}$ could be calculated

$$\boldsymbol{z}_{j,k} = \boldsymbol{S}_j\boldsymbol{W}_j^{-\frac{1}{2}}\boldsymbol{T}_j^T(\boldsymbol{q}_k - \tilde{\boldsymbol{q}}_{j,k}) \tag{23a}$$

$$\boldsymbol{T}_j\boldsymbol{W}_j\boldsymbol{T}_j^T = \tilde{\boldsymbol{Q}}'_{j,k} \tag{23b}$$

$$\boldsymbol{S}_j\boldsymbol{W}_j^{\frac{1}{2}}\boldsymbol{T}_j^T\phi_{j,k} = \begin{bmatrix}\left(\phi_{j,k}^T\tilde{\boldsymbol{Q}}'_{j,k}\phi_{j,k}\right)^{\frac{1}{2}} & 0 & \cdots & 0\end{bmatrix}^T \tag{23c}$$

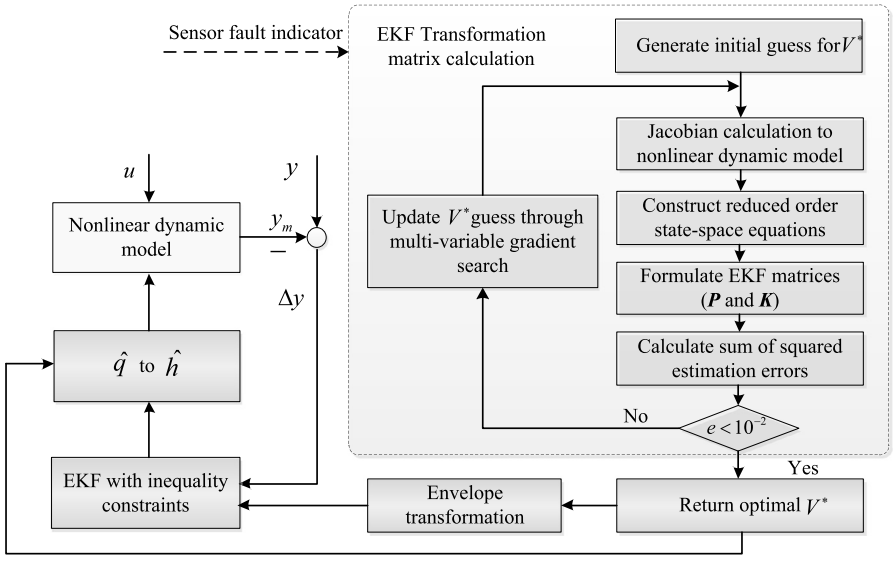

Fig. 3. Flowchart of the resultant EKF algorithm for gas turbine engine health monitoring.

where $\boldsymbol{T}_j$ is orthogonal, $\boldsymbol{W}_j$ is diagonal (the quantities of matrices $\boldsymbol{T}_j$ and $\boldsymbol{W}_j$ can be derived from the Jordan canonical decomposition of $\tilde{\boldsymbol{Q}}'_{j,k}$). Since the matrix $\boldsymbol{W}_j$ is diagonal, $\boldsymbol{W}_j^{1/2}$ says the square root of every diagonal element of $\boldsymbol{W}_j$. The matrix $\boldsymbol{S}_j$ is generated by Gram–Schmidt orthogonalization [40] to find the orthogonal $\boldsymbol{S}_j$ following Eq. (23c). In the initialization of resultant EKF, the mean and covariance of tuner equal to those without inequality constraint, i.e. $\tilde{\boldsymbol{q}}_{j,k} = \hat{\boldsymbol{q}}_k$, $\tilde{\boldsymbol{Q}}'_{j,k} = \boldsymbol{Q}'_k$, $j = 0$. The constraints are in turn decoupled, and there are m transformed constrain inequalities yielded with each constraints related to one transformed state. Based on the definitions in Eq. (23), the lower bound in Eq. (22) is rewritten as

$$\begin{aligned}
&\phi_{j,k}^T \boldsymbol{q}_k \geq \boldsymbol{c}_{j,k} \\
&\phi_{j,k}^T \boldsymbol{T}_j \boldsymbol{W}_j^{\frac{1}{2}} \boldsymbol{S}_j^T \boldsymbol{z}_{j,k} + \phi_{j,k}^T \tilde{\boldsymbol{q}}_{j,k} \geq \boldsymbol{c}_{j,k} \\
&\frac{\phi_{j,k}^T \boldsymbol{T}_j \boldsymbol{W}_j^{\frac{1}{2}} \boldsymbol{S}_j^T \boldsymbol{z}_{j,k}}{(\phi_{j,k}^T \tilde{\boldsymbol{Q}}'_{j,k} \phi_{j,k})^{1/2}} \geq \frac{\boldsymbol{c}_{j,k} - \phi_{j,k}^T \tilde{\boldsymbol{q}}_{j,k}}{(\phi_{j,k}^T \tilde{\boldsymbol{Q}}'_{j,k} \phi_{j,k})^{1/2}} \\
&[1, 0, \cdots, 0] \boldsymbol{z}_{j,k} \geq \frac{\boldsymbol{c}_{j,k} - \phi_{j,k}^T \tilde{\boldsymbol{q}}_{j,k}}{(\phi_{j,k}^T \tilde{\boldsymbol{Q}}'_{j,k} \phi_{j,k})^{1/2}}
\end{aligned} \tag{24}$$

The upper bound can be obtained in the similar way as Eq. (24), then the former j inequality constraints are normalized

$$\begin{aligned}
&\boldsymbol{l}_{j,k} \leq [1, 0, \cdots, 0] \boldsymbol{z}_{j,k} \leq \boldsymbol{m}_{j,k} \\
&\boldsymbol{l}_{j,k} = \frac{\boldsymbol{c}_{j,k} - \phi_{j,k}^T \tilde{\boldsymbol{q}}_{j,k}}{(\phi_{j,k}^T \tilde{\boldsymbol{Q}}'_{j,k} \phi_{j,k})^{1/2}} \\
&\boldsymbol{m}_{j,k} = \frac{\boldsymbol{d}_{j,k} - \phi_{j,k}^T \tilde{\boldsymbol{q}}_{j,k}}{(\phi_{j,k}^T \tilde{\boldsymbol{Q}}'_{j,k} \phi_{j,k})^{1/2}}
\end{aligned} \tag{25}$$

Since $\boldsymbol{z}_{j,k}$ has statistically independent element, only the first element is constrained in Eq. (25) and the PDF truncation reduces to a one-dimensional PDF. The part falling outside the constraint bound is removed due to $\boldsymbol{z}_{j,k}$ lying between $\boldsymbol{l}_{j,k}$ and $\boldsymbol{m}_{j,k}$. The truncated PDF is normalized and the probability sum within constraint bound equals to one. The mean μ_j and variance σ_j^2 of the first element of $\boldsymbol{z}_{j,k}$ with the constraint enforcement are expressed

$$\begin{aligned}
&\alpha = \frac{\sqrt{2}}{\sqrt{\pi}(erf(\boldsymbol{m}_{j,k}/\sqrt{2}) - erf(\boldsymbol{l}_{j,k}/\sqrt{2}))} \\
&\mu_j = \alpha \int_{c_{j,k}}^{d_{j,k}} \xi \exp(-\xi^2/2) d\xi = \alpha\left[\exp(-\boldsymbol{l}_{j,k}^2/2) - \exp(-\boldsymbol{m}_{j,k}^2/2)\right] \\
&\sigma_j^2 = \alpha \int_{c_{j,k}}^{d_{j,k}} (\xi - \mu_j)^2 \exp(-\xi^2/2) d\xi \\
&\quad = \alpha\left[\exp(-\boldsymbol{l}_{j,k}^2/2)(\boldsymbol{l}_{j,k} - 2\mu_j)\right. \\
&\qquad \left. - \exp(-\boldsymbol{m}_{j,k}^2/2)(\boldsymbol{m}_{j,k} - 2\mu_j)\right] + \mu_j^2 + 1
\end{aligned} \tag{26}$$

where α is a magnification factor, and $erf(t) = \frac{2}{\sqrt{\pi}} \int_0^t \exp(-\tau^2) d\tau$. The inverse transformation of Eq. (23) is conducted, and the mean and covariance of the constrained tuner estimate are achieved

$$\begin{aligned}
&\tilde{\boldsymbol{q}}_{j+1,k} = \boldsymbol{T}_j \boldsymbol{W}_j^{1/2} \boldsymbol{S}_j^T [\mu_j, 0, \cdots, 0]^T + \tilde{\boldsymbol{q}}_{j,k} \\
&\tilde{\boldsymbol{Q}}'_{j+1,k} = \boldsymbol{T}_j \boldsymbol{W}_j^{1/2} \boldsymbol{S}_j^T diag(\sigma_j^2, 1, \cdots, 1) \boldsymbol{S}_j \boldsymbol{W}_j^{1/2} \boldsymbol{T}_j^T
\end{aligned} \tag{27}$$

Repeat the steps from Eq. (23) to Eq. (27) to enforce the next constraint to the state estimate and jump out of the iteration until $j = m$. For example, $\tilde{\boldsymbol{q}}_{0,k}$ is the state estimate without any constraints, and $\tilde{\boldsymbol{q}}_{3,k}$ is the state estimate with the first three constraints. Since the inequality constraints are independent, the mean and variance of the tuner with all constraints can be calculated after repeating process m times. For gas turbine engine health monitoring, the resultant EKF to the issue of underdetermined estimation with inequality constraints is detailed shown in Fig. 3.

4. Experiments and analysis

Experiments are carried out on a semi-physical platform of turbojet engine that is developed by Nanjing University of Aeronautics and Astronautics [28,29], and then a systematical discussion is presented to reveal the performance of the proposed methodology. The involved state estimation algorithms run in Matlab Software, and the engine operates at the maximum power in typical flight regions. The maximum power operation is defined as the corrected low pressure rotor speed $N_{L,cor} = 1$. Turbojet engine sensor measurements, nominal value and standard deviation are shown in Table 2 [26,41].

Table 2
Turbojet engine sensor measurements, nominal value and standard deviation.

Measurement	Acronyms	Nominal value	Standard deviation
Low pressure spool speed	N_L	1	0.0015
High pressure spool speed	N_H	1	0.0015
LPC outlet pressure	P_{25}	1	0.0015
HPC outlet pressure	P_3	1	0.0015
HPT outlet pressure	P_{45}	1	0.0015
HPT outlet temperature	T_{45}	1	0.002
LPT outlet pressure	P_6	1	0.0015
LPT outlet temperature	T_6	1	0.002

Table 3
Turbojet engine gas path performance fault cases.

Case	Variations of health parameter	Abnormal component
I	ΔSE_1 −0.4%	LPC
II	ΔSE_2 −0.7% and ΔSW_2 −1%	HPC
III	ΔSE_2 −1%	
IV	ΔSW_2 −1%	
V	ΔSW_3 +1%	HPT
VI	ΔSE_3 −1% and ΔSW_3 −1%	
VII	ΔSE_3 −1%	
VIII	ΔSE_4 −1%	LPT
IX	ΔSE_4 −0.6% and ΔSW_4 +1%	

The element of health parameter vector $\boldsymbol{h}$ is initialized to the nominal value equaling 1. The health parameters derive from the normal values suddenly in the performance fault, and the shift quantities of various fault cases are presented in Table 3 [31]. The turbojet engine operating data are collected and corrected through similar normalized process before the utilization for health monitoring.

The underdetermined estimation using various sensor subsets are performed, and the effects of different sensed information and prior knowledge to estimation accuracy are analyzed. The robustness of the resultant EKF at the maximum power in typical flight region is discussed. In order to compare the estimation performance of the examined methodologies, two performance indices, viz. root mean square error (*ME*) and standard square error (*SD*) are defined and given in the following forms, where the sampling number is S.

$$ME = \left[\frac{1}{S}\sum_{k=1}^{S}\left(\Delta\hat{\boldsymbol{h}}(k) - \Delta\boldsymbol{h}(k)\right)^T\left(\Delta\hat{\boldsymbol{h}}(k) - \Delta\boldsymbol{h}(k)\right)\right]^{1/2}$$
$$SD = \frac{1}{n}\left[\frac{1}{S-1}\sum_{k=1}^{S}\left(\Delta\hat{\boldsymbol{h}}(k) - \frac{1}{S}\sum_{k=1}^{S}\Delta\hat{\boldsymbol{h}}(k)\right)^T \times \left(\Delta\hat{\boldsymbol{h}}(k) - \frac{1}{S}\sum_{k=1}^{S}\Delta\hat{\boldsymbol{h}}(k)\right)\right]^{1/2} \quad (28)$$

4.1. Fault detection with gas path benchmark data

Nine benchmark data sets about engine performance fault modes referred to Table 3 are used to compare health monitoring performance of the basic EKF, moving horizon state estimation (MHE), underdetermined EKF and resultant EKF. The engine operating points in the flight envelope are the ground international standard atmosphere (ISA) operation (Scenario 1: $H = 0$, $Ma = 0$, $W_f = 1.15$ kg/s, $A_8 = 0.2083$ m^2) and the high altitude operation (Scenario 2: $H = 10700$ m, $Ma = 0.84$, $W_f = 0.517$ kg/s, $A_8 = 0.2083$ m^2). The simulation time is totally 50 seconds and the health parameter shifts are injected into the nominal engine model at 10 seconds. The sensor P_3 failure is simulated. The number of available measurement is seven and the count of health parameters to be estimated is eight. As was mentioned earlier, the underdetermined EKF and resultant EKF could estimate all state variables while the basic EKF is disabled in underdetermined estimation.

In order to fulfill the comparison, the LPT flow capacity ΔSW_4 is assumed known and equals to 1 in the basic EKF since the change quantity of ΔSW_4 is the least among all health parameters in Table 2. It implies that the engine fault case IX in Table 3 can't be detected by the basic EKF. The system process noise covariance $\boldsymbol{Q}$ is generated from the several tests, i.e. $\boldsymbol{Q} = 0.004 \times \boldsymbol{I}_{8\times 8}$, and the diagonal elements of measurement noise covariance $\boldsymbol{R}$ are referred to Table 2. Based on the procedure of resultant EKF algorithm given in Fig. 3, the transformation matrices of resultant EKF at the typical operating points, i.e. Scenario 1 denoted by $\boldsymbol{V}_1^*$ and Scenario 2 denoted by $\boldsymbol{V}_2^*$, are separately worked out. The Frobenius norms of both $\boldsymbol{V}_1^*$ and $\boldsymbol{V}_2^*$ equal one, and their condition number are 33.81 and 34.18. Then we can find that these transformation matrices are steady at the typical operating condition.

The eight health parameters are obtained from the tuning vector $\boldsymbol{q}$ with help of the optimal transformation matrix both in the underdetermined EKF and resultant EKF, while seven health parameters except for ΔSW_4 worked out in the basic EKF. The *ME*s of health parameter estimates for nine benchmark data sets related to general performance fault in two Scenarios are presented in Table 4. The performance index ME_{av} by each method is the average of *ME* in all involved fault cases.

As it can be seen from Table 4, the estimation errors of the underdetermined EKF are the largest among the examined algorithms in the most fault cases. The *ME*s by the MHE and underdetermined EKF are larger than 3.5e−2 (the threshold of performance fault [32]) in some cases, and the detection results are unacceptable. The *ME*s by the resultant EKF are all below 3.5e−2 and far smaller than those by the MHE and the underdetermined EKF, and the performance of resultant EKF is nearly the same as the basic EKF from the case I to case VIII. The known state information is considered to compensate partial measurement absence in the resultant EKF, and it makes the estimation accuracy of resultant EKF better than that of underdetermined EKF. We can also find that the *ME*s at ground ISA by all state estimation methods are less than that at

Table 4
*ME*s for benchmark data sets corresponding to engine gas path fault cases ($\times 10^{-2}$).

Operating points	Algorithms	Case									ME_{av}
		I	II	III	IV	V	VI	VII	VIII	IX	
Scenario 1	Basic EKF	1.30	1.93	2.34	1.41	1.27	1.37	1.28	2.28	–	1.95
	MHE	1.78	2.15	3.19	2.50	2.00	3.13	2.43	3.09	2.12	2.48
	Underdetermined EKF	2.49	3.12	3.37	2.58	2.82	2.88	2.56	3.45	3.10	2.93
	Resultant EKF	1.42	1.91	2.24	2.63	1.73	1.70	1.29	2.23	2.49	1.96
Scenario 2	Basic EKF	2.79	2.16	2.54	1.80	1.53	2.16	1.04	2.23	–	2.03
	MHE	2.30	3.84	3.17	4.36	2.33	3.24	2.67	3.39	3.37	3.18
	Underdetermined EKF	2.97	4.07	4.11	3.57	3.12	3.13	2.69	3.67	3.25	3.40
	Resultant EKF	1.46	2.18	2.41	1.67	2.72	2.25	2.39	2.38	2.51	2.22

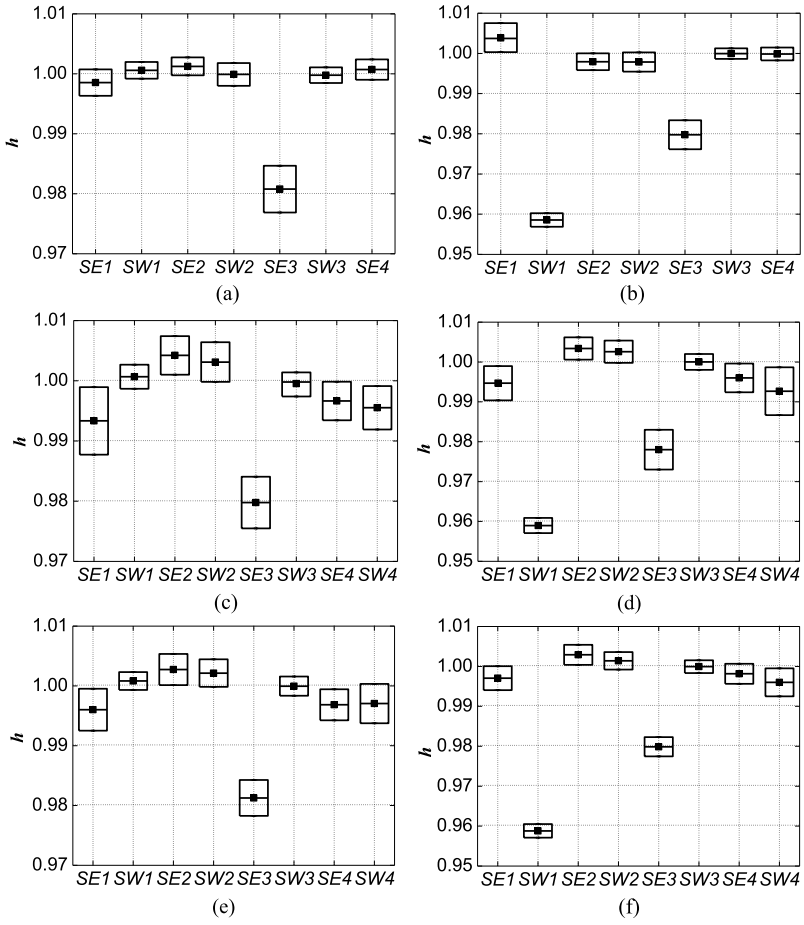

Fig. 4. The mean, maximum and minimum of each health parameter estimates at the ground design point. (a) Basic EKF in the case of SE_3 −2%, (b) Basic EKF in the case of SW_1 −4% and SE_3 −2%, (c) Underdetermined EKF in the case of SE_3 −2%, (d) Underdetermined EKF in the case of SW_1 −4% and SE_3 −2%, (e) Resultant EKF in the case of SE_3 −2%, (f) Resultant EKF in the case of SW_1 −4% and SE_3 −2%.

the high altitude. Similar normalization process to the system parameters could extend the EKF application in flight envelope, but it also inevitably brings the estimation errors.

4.2. Gas path fault test-bed data monitoring

Two test-bed data sets which are collected from wet experiments at the ground design point are employed to further compare the performance of the examined EKF algorithms. These data sets including 500 samples refer to the following engine component fault cases: (1) −2% on SE_3, (2) −4% on SW_1 and −2% on SE_3. Sensor fault detection and isolation (FDI) logic addressed in [42,43] is implemented, and sensor P_3 failure is recognized and then this faulty measurement excluded from the available sensed vector. Fig. 4 gives the mean, maximum and minimum of each health parameter estimates by the three EKF algorithms, and color variations in turn represent the estimates of health parameters.

As can be seen from Fig. 4, the mean values of health parameter estimates by the basic EKF are closer to their actual values than those by the underdetermined EKF and resultant EKF, and change amplitudes of health parameter estimates by the basic EKF are almost the least. Furthermore, the performance indices *ME* and *SD* by the involved EKF algorithms for two test-bed data sets at the ground design point are presented in Table 5. The *ME* and *SD* also reveal that the underdetermined EKF performance is inferior to the other EKFs, and the performance of resultant EKF approaches to that of basic EKF. However, it is noted that ΔSW_4 is assumed to be constant and not estimated in the basic EKF, and wrong estimates of health parameter will be generated when the fault cases about ΔSW_4 occur. Consequently, the resultant EKF is the best way to achieve underdetermined estimation of engine health state with the sensor P_3 absence regards among these EKFs.

Table 5
*ME*s and *SD*s for two test-bed data sets at the ground design point ($\times 10^{-2}$).

Algorithms	Indices	SE_3 −2%	SW_1 −4% and SE_3 −2%
Basic EKF	*ME*	1.39	1.65
	SD	0.20	0.23
Underdetermined EKF	*ME*	2.76	2.84
	SD	0.34	0.32
Resultant EKF	*ME*	1.86	1.94
	SD	0.26	0.24

Fig. 5 and Fig. 6 detailed show the estimation results of health parameters by the resultant EKF in the fault cases of −2% on SE_3, and −4% on SW_1 and −2% on SE_3. The red lines are the actual health parameters and blue lines are their estimates. The deviation of the health parameters could be rapidly tracked around 2 s by the resultant EKF, and the estimates fluctuate within the small intervals in a long term. Both dynamic and steady estimation performance of the resultant EKF are satisfactory.

4.3. Health estimating robustness over operating envelope

The optimal transformation matrix $\boldsymbol{V}^*$ should be calculated at certain operating point before resultant EKF application. If this matrix is constant at different operating points in the flight envelope,

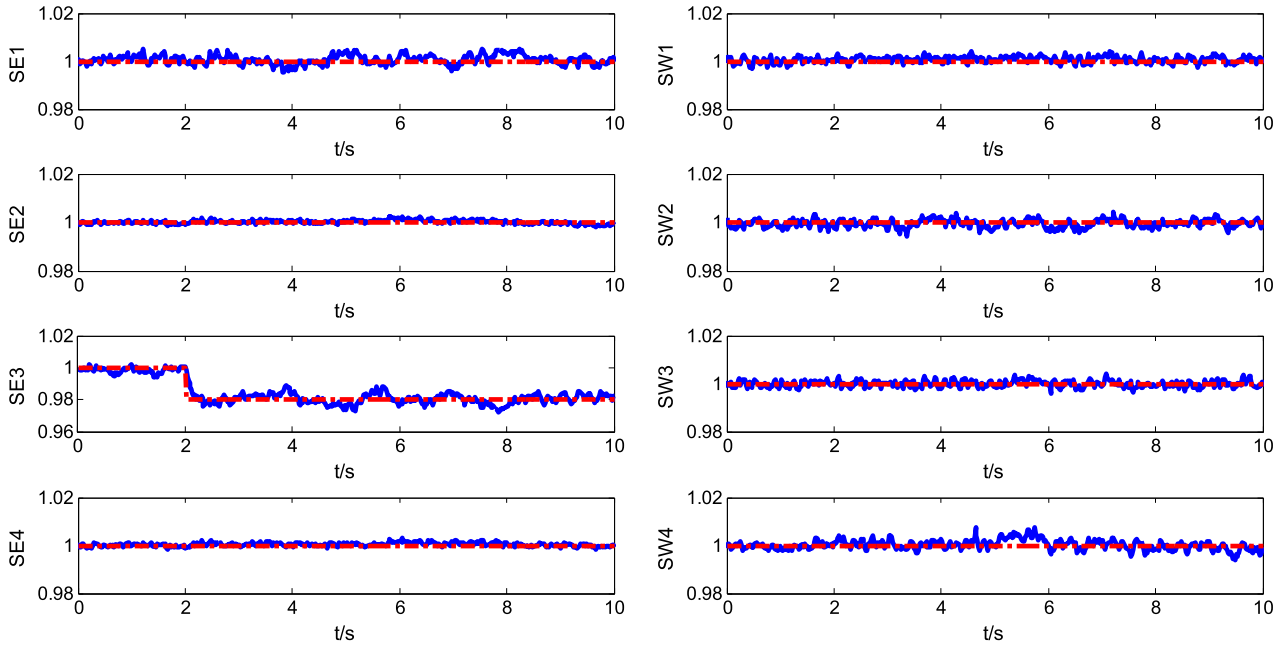

Fig. 5. The estimated values of health parameters by the resultant EKF in the case of SE_3 −2%. (For interpretation of the references to color in this figure, the reader is referred to the web version of this article.)

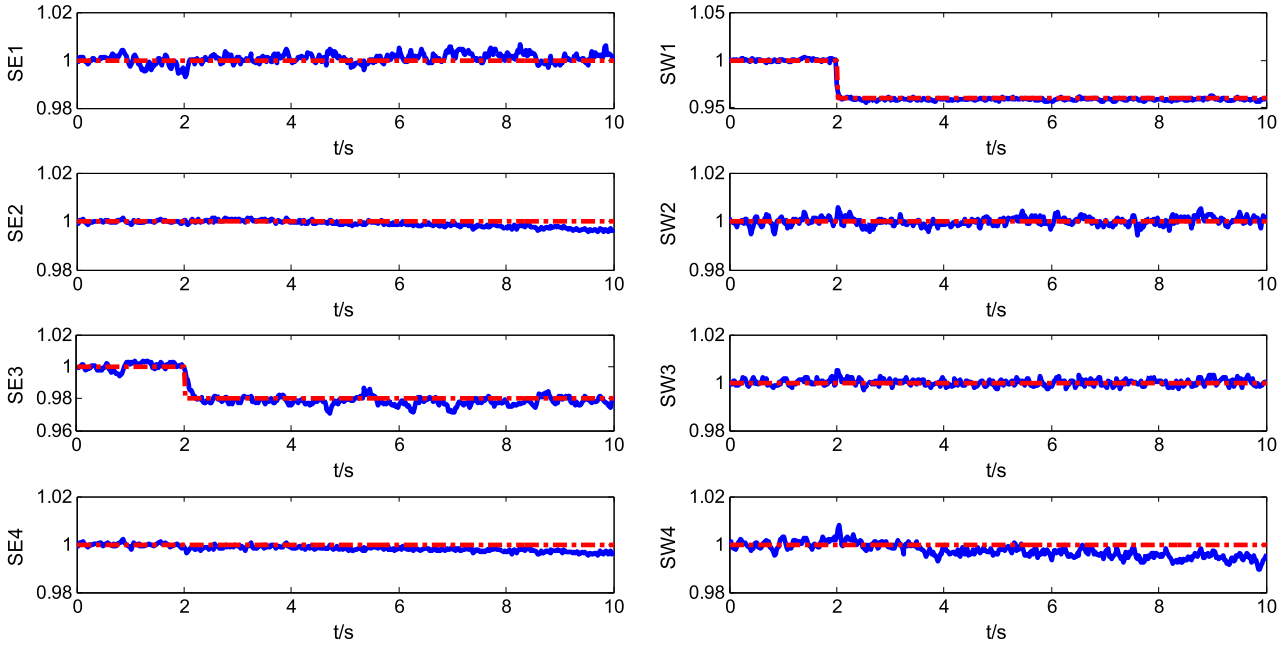

Fig. 6. The estimated values of health parameters by the resultant EKF in the case of SW_1 −4% and SE_3 −2%. (For interpretation of the references to color in this figure, the reader is referred to the web version of this article.)

it could obviously reduce computational efforts and save in-flight storage. Hence, the resultant EKF robustness to various operating points is discussed on the numerical simulation in this section, and a test operating point (Scenario 3: $H = 5000$ m, $Ma = 0.8$, $W_f = 0.93$ kg/s, $A_8 = 0.2083$ m^2) is introduced which falls into the region between Scenario 1 and Scenario 2. Three operating points of the engine are all at the maximum power $N_{L,cor} = 1$. The optimal transformation matrix $\boldsymbol{V}_3^*$ is calculated using the Scenario 1 data and Scenario 2 data with the same weight. The condition number of $\boldsymbol{V}_3^*$ is 18.79, and it implies that the transformation from the original health parameter to tuner is steady at the maximum power.

Table 6 shows that the *ME*s of health parameter estimates vary with different transformation matrices. The optimal matrices $\boldsymbol{V}_1^*$ and $\boldsymbol{V}_2^*$, which are separately obtained at ground operation Scenario 1 and high altitude operation Scenario 2, produce satisfactory performance at their own operation points. The *ME* using $\boldsymbol{V}_1^*$ is 1.86e−02 at Scenario 1, 2.83 at Scenario 2, and 2.67 at Scenario 3, while the *ME*s using $\boldsymbol{V}_3^*$ at three Scenarios are separately 2.13, 2.25 and 2.18 in Table 6. Therefore, the *ME* using $\boldsymbol{V}_1^*$ is 0.27e−02 less than the *ME* using $\boldsymbol{V}_3^*$ in the fault case SE_3 −2% at the ground operation. But the *ME*s using $\boldsymbol{V}_1^*$ are separately 0.58e−02 and 0.49e−02 more than those using $\boldsymbol{V}_3^*$ at Scenario 2 and Scenario 3.

Table 6
MEs of health parameter estimates related to the various transformation matrices ($\times 10^{-2}$).

Transformation matrix	SE_3 −2%			SW_1 −4% and SE_3 −2%		
	Scenario 1	Scenario 2	Scenario 3	Scenario 1	Scenario 2	Scenario 3
$\boldsymbol{V}_1^*$	1.86	2.83	2.67	1.94	3.14	3.28
$\boldsymbol{V}_2^*$	2.76	1.91	2.63	3.12	2.36	3.24
$\boldsymbol{V}_3^*$	2.13	2.25	2.18	2.77	2.89	3.03

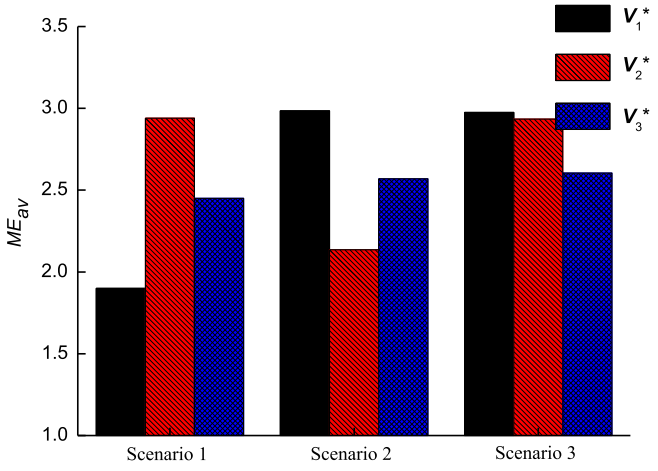

Fig. 7. ME_{av} of health parameter estimates related to $\boldsymbol{V}_1^*$, $\boldsymbol{V}_2^*$, and $\boldsymbol{V}_3^*$ at three operating points.

The performance index ME_{av} in the fault cases of −2% on SE_3, and −4% on SW_1 and −2% on SE_3 are presented in Fig. 7. The performance index ME_{av} using matrix $\boldsymbol{V}_3^*$ at Scenario 1 is not as good as that using $\boldsymbol{V}_1^*$, and also not good as that using $\boldsymbol{V}_2^*$ at Scenario 2. Nevertheless, the resultant EKF using $\boldsymbol{V}_3^*$ produces the relatively smooth ME_{av} than the others, around 2.50e−2. Besides, there are no *MEs* exceeding 3.50e−02 at the maximum power in the examined flight region, and the estimation results of resultant EKF related to three optimal transformation matrices are acceptable. That is to say, the resultant EKF robustness to the typical operating points is satisfactory.

4.4. Health estimating performance comparisons by different measurement subset

In the experiments above, the resultant EKF is conducted given that all measurement used for state estimation except P_3. To further evaluate the performance of resultant EKF, we try to launch experiments utilizing various measurement subsets to estimate eight health parameters. The sensed signals N_L and N_H are the key parameters to represent the turbojet engine operation and are designed by double-channel redundancy. If one channel breaks down, the other channel would accommodate this fault and works [43]. The rest measured signals are collected using single channel. Hence, the measurements N_L and N_H failure is not considered in the study, and there are six combinations to construct seven measurements from the eight sensed signals. Since the *MEs* of health parameter estimates under the measurement subset $[N_L N_H P_{25} P_{45} T_{45} P_6 T_6]$ for benchmark data have been given in Table 4, Table 7 presents the *MEs* of the remaining measurement combinations at ground operation Scenario 1 and high altitude operation Scenario 2.

As can be seen from Table 4 and Table 7, the resultant EKF using available sensed subsets $[N_L N_H P_{25} P_3 P_{45} T_{45} P_6]$ and $[N_L N_H P_{25} P_3 P_{45} T_{45} T_6]$ produce larger ME_{av} than that using other sensor subsets both at the ground and high altitude operations. The performance index ME_{av} under the sensor subset $[N_L N_H P_3 P_{45} T_{45} P_6 T_6]$ is the least. It implies that the sensors T_6 and P_6 are another two important measurements for health estimation, and the estimation errors evidently increase as the loss of T_6 or P_6. Sensor significance for turbojet engine health estimation can also be obtained from the ME_{av} sequence in Table 7. Tests about eight health parameters estimation using six measurements are performed, and the *MEs* of health parameter estimates for benchmark data as two sensors absence are presented in Table 8.

In Table 8, the *MEs* in several fault cases are less than 3.5e−2, and the resultant EKF could still give acceptable results for engine health monitoring. However, the performance of the resultant EKF becomes worse in general as one more measurement unavailable. The ME_{av} by resultant EKF using the sensor subset $[N_L N_H P_{25} P_3 P_{45} T_{45}]$ is the largest among all six-sensor combinations. It indicates that the measurements without P_6 and T_6 will produce more estimation errors in the engine health monitoring. It also could give us a guideline that the sensors, especially P_6 and T_6, should preferably be collected by double channel redundancy technique.

5. Conclusion

This paper has proposed an improved nonlinear state estimation approach to gas turbine engine health monitoring. The novelty

Table 7
MEs for benchmark data as one sensor absence ($\times 10^{-2}$). Available measurement subsets label 1 to 5 are $[N_L N_H P_3 P_{45} T_{45} P_6 T_6]$, $[N_L N_H P_{25} P_3 T_{45} P_6 T_6]$, $[N_L N_H P_{25} P_3 P_{45} P_6 T_6]$, $[N_L N_H P_{25} P_3 P_{45} T_{45} T_6]$, $[N_L N_H P_{25} P_3 P_{45} T_{45} P_6]$, respectively.

Operating points	Sensor subset	Case									ME_{av}	False positive
		I	II	III	IV	V	VI	VII	VIII	IX		
Scenario 1	1	1.46	1.65	2.10	1.45	1.17	1.29	1.30	2.06	1.67	1.57	0/9
	2	1.15	1.64	2.98	1.66	2.00	2.79	1.33	2.69	2.35	2.07	0/9
	3	1.46	1.68	3.21	2.21	2.06	2.77	2.03	2.43	2.12	2.22	0/9
	4	1.27	1.35	3.35	2.16	2.50	3.88	1.66	2.49	2.12	2.31	1/9
	5	1.40	2.46	2.97	3.40	2.36	2.42	1.36	2.17	2.18	2.30	0/9
Scenario 2	1	1.28	1.84	2.83	1.70	1.69	2.68	2.01	2.42	1.74	2.02	0/9
	2	1.32	1.90	2.89	1.65	1.61	3.20	2.05	2.02	1.68	2.04	0/9
	3	1.46	1.74	3.62	2.21	2.44	3.02	1.51	2.73	2.59	2.37	1/9
	4	1.40	2.50	2.83	2.22	2.47	3.82	2.84	2.66	2.42	2.57	1/9
	5	1.56	2.64	3.45	2.87	2.58	3.14	2.40	2.25	2.90	2.64	0/9

Table 8
*ME*s for benchmark data sets as two sensors absence at scenario 1 ($\times 10^{-2}$).

Absent sensors	Case									ME_{av}	False positive
	I	II	III	IV	V	VI	VII	VIII	IX		
P_6, T_6	**2.03**	**6.29**	**15.36**	**27.60**	**2.41**	**5.56**	**7.79**	**8.10**	**4.49**	**8.85**	**7/9**
P_{45}, P_6	2.46	3.48	2.86	3.65	5.12	3.36	6.50	2.51	4.41	3.82	4/9
P_{45}, T_6	1.41	2.85	4.13	4.55	2.59	2.65	2.22	4.32	3.70	3.16	4/9
T_{45}, P_6	1.02	2.41	2.51	1.76	5.02	4.30	4.71	2.11	1.77	2.85	3/9
T_{45}, T_6	4.98	5.57	3.64	3.57	12.53	31.21	2.09	2.20	4.30	7.79	7/9
T_{45}, P_{45}	1.61	1.84	2.59	1.55	2.12	2.74	1.53	2.00	4.28	2.25	1/9
P_3, P_6	1.49	2.03	1.92	1.89	2.68	3.38	1.66	2.10	2.35	2.17	0/9
P_3, T_6	1.91	2.99	4.21	3.81	2.81	4.14	1.98	4.53	2.99	3.26	4/9
P_3, P_{45}	1.89	3.16	4.74	3.89	5.35	6.35	1.85	4.28	3.69	3.91	6/9
P_3, T_{45}	1.16	2.30	3.03	2.05	2.91	3.67	1.84	2.04	2.52	2.39	1/9
P_{25}, P_6	2.58	1.89	3.89	3.46	15.21	4.50	16.38	3.38	11.20	6.94	5/9
P_{25}, T_6	2.30	2.44	2.91	3.71	3.36	3.16	4.23	2.04	2.37	2.95	2/9
P_{25}, P_{45}	1.40	2.33	2.43	1.75	1.95	2.93	2.06	2.08	1.78	2.08	0/9
P_{25}, T_{45}	1.40	3.10	1.94	3.35	3.40	2.44	2.56	3.64	7.11	3.22	2/9
P_{25}, P_3	1.78	2.32	4.77	4.33	6.75	5.92	1.77	4.88	4.50	4.11	6/9

of this methodology lies in the development of resultant EKF algorithm with inequality constraints for the purpose of underdetermined estimation. The tuner with reduced order is introduced into the underdetermined EKF using the optimal transformation matrix, and it is a linear combination of state variables. The resultant EKF is a new uncertainty estimator that inequality constraints are combined to underdetermined EKF. One advantage of this methodology is that this improved EKF can deal with underdetermined estimation for nonlinear dynamic system. The EKF in state estimation applications is no longer restricted by the condition that available measurement number is less than the count of state variables. Another advantage of this methodology is that the underdetermined estimation accuracy is improved, since prior state information depicted by inequality constraints is considered and used to make up for partial measurement absence. Important theoretical algorithms of the resultant EKF have been presented to the issue of nonlinear underdetermined state estimation with inequality constraints.

The methodology is tested and validated using benchmark data and test-bed data of a turbojet engine. The experimental results of health monitoring by the basic EKF, underdetermined EKF and resultant EKF are compared at the typical operating points. Both of the underdetermined EKF and resultant EKF achieve eight health parameter estimation using seven sensors at the ground and high altitude operations, while the basic EKF fails to accomplish it. The resultant EKF is superior to underdetermined EKF with regards to estimation accuracy. In addition, the resultant EKF estimation robustness to various measurement subsets at the maximum power in the typical flight regions is satisfactory. The resultant EKF estimator is easy to design, and by this estimator the engine health monitoring results are acceptable as one sensor is absent. However, the estimation accuracy of the methodology decreases as two measurements become unavailable, and it can't work well especially in the case that both sensors P_6 and T_6 failure occurs. The methodology developed in this paper is not limited to turbojet engine health monitoring, but also can be extended to other engine types and applied to fault tolerant control.

This research establishes a new direction in state estimation for nonlinear dynamic system by proposing an improved nonlinear state estimator technique that is beneficial for gas turbine engine health monitoring applications. There are several important topics for future research that are related to this work. First, further studies can be done to investigate the performance when the prior measurement information is supplemented and estimation errors performance index changes. Except for the prior knowledge of state variables in this study, the known measurement information could also be used as the constraints of nonlinear estimator. The weights of mean bias and square deviation to the performance index of estimation errors in the resultant EKF could be tuned to various estimation tasks. Second, although this paper focuses on turbojet engine health monitoring at the maximum operating power in typical flight region, extensions to the cases that have more operational conditions in whole flight envelope are worthy of further exploration.

Conflict of interest statement

The authors declare that they do not have any conflicts of interest to this work.

Acknowledgements

We are grateful for the financial support of the National Natural Science Foundation of China (No. 61304133), and China Outstanding Postdoctoral Science Foundation (No. 2015T80552). Gratitude is also extended to Professor Viliam Makis for useful advices and to China Scholarship Council (No. 201506835001) for supporting the first author to carry out collaborative research in the Department of Mechanical and Industrial Engineering at the University of Toronto. Moreover, the authors wish to thank the anonymous reviewers for their constructive comments and great help in the writing process, which will improve the manuscript significantly.

References

[1] A.J. Volponi, Gas turbine engine health management: past, present, and future trends, J. Eng. Gas Turbines Power 136 (5) (2014) 051201.
[2] M.A. Zaidana, R. Relan, A.R. Mills, R.F. Harrison, Prognostics of gas turbine engine: an integrated approach, Expert Syst. Appl. 42 (22) (2015) 8472–8483.
[3] K.B. Liu, S. Huang, Integration of data fusion methodology and degradation modeling process to improve prognostics, IEEE Trans. Autom. Sci. Eng. 13 (1) (2016) 344–354.
[4] N. Aretakis, I. Roumeliotis, A. Alexiou, C. Romesis, K. Mathioudakis, Turbofan engine health assessment from flight data, J. Eng. Gas Turbines Power 137 (4) (2015) 041203.
[5] R.H. Luppold, J.R. Roman, G.W. Gallops, L.J. Keer, Estimating in-flight engine performance variations using Kalman filter concepts, AIAA-89-2584.
[6] B. Pourbabaee, N. Meskin, K. Khorasani, Sensor fault detection, isolation, and identification using multiple-model-based hybrid Kalman filter for gas turbine engines, IEEE Trans. Control Syst. Technol. 24 (4) (2016) 1184–1200.
[7] Y.G. Li, T. Korakianitis, Improved multiple point nonlinear genetic algorithm based performance adaptation using least square method, J. Eng. Gas Turbines Power 134 (3) (2012) 031701.
[8] M.A. Zaidan, R.F. Harrison, A.R. Mills, P.J. Fleming, Bayesian hierarchical models for aerospace gas turbine engine prognostics, Expert Syst. Appl. 42 (1) (2015) 539–553.
[9] M.A. Zaidan, A.R. Mills, R.F. Harrison, P.J. Fleming, Gas turbine engine prognostics using Bayesian hierarchical models: a variational approach, Mech. Syst. Signal Process. 70–71 (2016) 120–140.
[10] R.B. Joly, S.O.T. Ogaji, R. Singh, S.D. Probert, Gas-turbine diagnostics using artificial neural-networks for a high bypass ratio military turbofan engine, Appl. Energy 78 (4) (2004) 397–418.

[11] S.S. Tayarani-Bathaie, K. Khorasani, Fault detection and isolation of gas turbine engines using a bank of neural networks, J. Process Control 36 (12) (2015) 22–41.
[12] E. Mohammadi, M. Montazeri-Gh, A fuzzy-based gas turbine fault detection and identification system for full and part-load performance deterioration, Aerosp. Sci. Technol. 46 (1) (2015) 82–93.
[13] S. Borguet, M. Henriksson, T. McKelvey, O. Leonard, A study on engine health monitoring in the frequency domain, J. Eng. Gas Turbines Power 133 (8) (2011) 081604.
[14] D. Dimogianopoulos, J. Hios, S. Fassois, Aircraft engine health management via stochastic modelling of flight data interrelations, Aerosp. Sci. Technol. 16 (1) (2012) 70–81.
[15] S. Sarkar, S. Sarkar, K. Mukherjee, A. Ray, A. Srivastav, Multi-sensor information fusion for fault detection in aircraft gas turbine engines, Proc. Inst. Mech. Eng., G J. Aerosp. Eng. 272 (12) (2013) 1988–2001.
[16] F. Lu, Y.Q. Lv, J.Q. Huang, X.Q. Qiu, A model-based approach for gas turbine engine performance optimal estimation, Asian J. Control 15 (6) (2013) 1794–1808.
[17] J.B. Armstrong, D.L. Simon, Implementation of an integrated on-board aircraft engine diagnostic architecture, NASA/TM-2012-217279.
[18] J.G. Sun, V. Vasilyev, B. Ilyasov, Advanced Multivariable Control Systems of Aeroengines, Beihang Press, Beijing, China, 2005, pp. 60–83.
[19] D. Simon, A comparison of filtering approaches for aircraft engine health estimation, Aerosp. Sci. Technol. 12 (2008) 276–284.
[20] D.L. Simon, S. Garg, Optimal tuner selection for Kalman filter-based aircraft engine performance estimation, NASA/TM-2010-216076.
[21] J.S. Litt, An optimal orthogonal decomposition method for Kalman filter-based turbofan engine thrust estimation, NASA/TM-2005-213864.
[22] M. Badami, P. Nuccio, A. Signoretto, Experimental and numerical analysis of a small-scale turbojet engine, Energy Convers. Manag. 76 (1) (2013) 225–233.
[23] M. Henriksson, T. Gronstedt, C. Breitholtz, Model-based on-board turbofan thrust estimation, Control Eng. Pract. 19 (6) (2011) 602–610.
[24] A. Jonathan, S. Jonathan, K. Dean, A modular aero-propulsion system simulation of a large commercial aircraft engine, in: 44th AIAA/ASME/SAE/ASEE Joint Propulsion Conference & Exhibit, AIAA-2008-4579.
[25] T. Nada, Performance characterization of different configurations of gas turbine engines, Propuls. Power Res. 3 (3) (2014) 121–132.
[26] F. Lu, Y. Chen, J.Q. Huang, D.D. Zhang, An integrated nonlinear model-based approach to gas turbine engine sensor fault diagnostics, Proc. Inst. Mech. Eng., G J. Aerosp. Eng. 228 (11) (2014) 2007–2021.
[27] Wadhah Hussein Abdul Razzaq Al-Doori, Parametric performance of gas turbine power plant with effect intercooler, Mod. Appl. Sci. 5 (3) (2011) 173–184.
[28] W.X. Zhou, Research on object-oriented modeling and simulation for aeroengine and control system, PhD thesis, Nanjing University of Aeronautics and Astronautics, Nanjing, China, 2007.
[29] F. Lu, W.H. Zheng, J.Q. Huang, M. Feng, Life cycle performance estimation and in-flight health monitoring for gas turbine engine, J. Dyn. Syst. Meas. Control 138 (9) (2016) 091009.
[30] A. Saxena, K. Goebel, D. Simon, N. Eklund, Damage propagation modeling for aircraft engine run-to-failure simulation, in: IEEE International Conference on Prognostics and Health Management, 2008, Oct. 6–9, Denver, CO, USA.
[31] S. Borguet, O. Leonard, Comparison of adaptive filters for gas turbine performance monitoring, J. Comput. Appl. Math. 234 (7) (2010) 2202–2212.
[32] H.F. Ju, Nonlinear filtering methods of gas path fault diagnosis for aeroengine, Master thesis, Nanjing University of Aeronautics and Astronautics, Nanjing, China, 2015.
[33] M.D. Espana, G.B. Gilyard, On the estimation algorithm used in adaptive performance optimization of turbofan engines, in: AIAA Joint Propulsion Conference, 1993, Jun. 28–Jul. 1, Monterey, CA, USA.
[34] D.L. Simon, J.B. Armstrong, An integrated approach for aircraft engine performance estimation and fault diagnostics, J. Eng. Gas Turbines Power 135 (7) (2013) 071203.
[35] B. Boulkroune, M. Darouach, M. Zasadzinski, Moving horizon state estimation for linear discrete-time singular systems, IET Control Theory Appl. 4 (3) (2010) 339–350.
[36] D. Simon, Kalman filtering with state constraints: a survey of linear and nonlinear algorithms, IET Control Theory Appl. 4 (8) (2010) 1303–1318.
[37] J. De Geeter, H. Brussel, A smoothly constrained Kalman filter, IEEE Trans. Pattern Anal. Mach. Intell. 19 (10) (1997) 1171–1177.
[38] D. Simon, D.L. Simon, Constrained Kalman filtering via density function truncation for turbofan engine health estimation, Int. J. Syst. Sci. 41 (2) (2010) 159–171.
[39] D. Simon, T. Chia, Kalman filtering with state equality constraints, IEEE Trans. Aerosp. Electron. Syst. 38 (1) (2002) 128–136.
[40] T.K. Moon, W.C. Stirling, Mathematical Methods and Algorithms for Signal Processing, Prentice Hall, Upper Saddle River, New Jersey, ISBN 0201361868, 2000.
[41] R. Ganguli, Noise and outlier removal from jet engine health monitoring signals using weighted FIR median hybrid filters, Mech. Syst. Signal Process. 16 (6) (2002) 967–978.
[42] J. Chen, R.J. Patton, Robust Model-Based Fault Diagnosis for Dynamic Systems, Kluwer Academic Publishers, Boston/Dordrecht/London, ISBN 0792384113, 2003.
[43] F. Lu, J.Q. Huang, Y.D. Xing, Fault diagnostics for turbo-shaft engine sensors based on a simplified on-board model, Sensors 12 (8) (2012) 11061–11076.